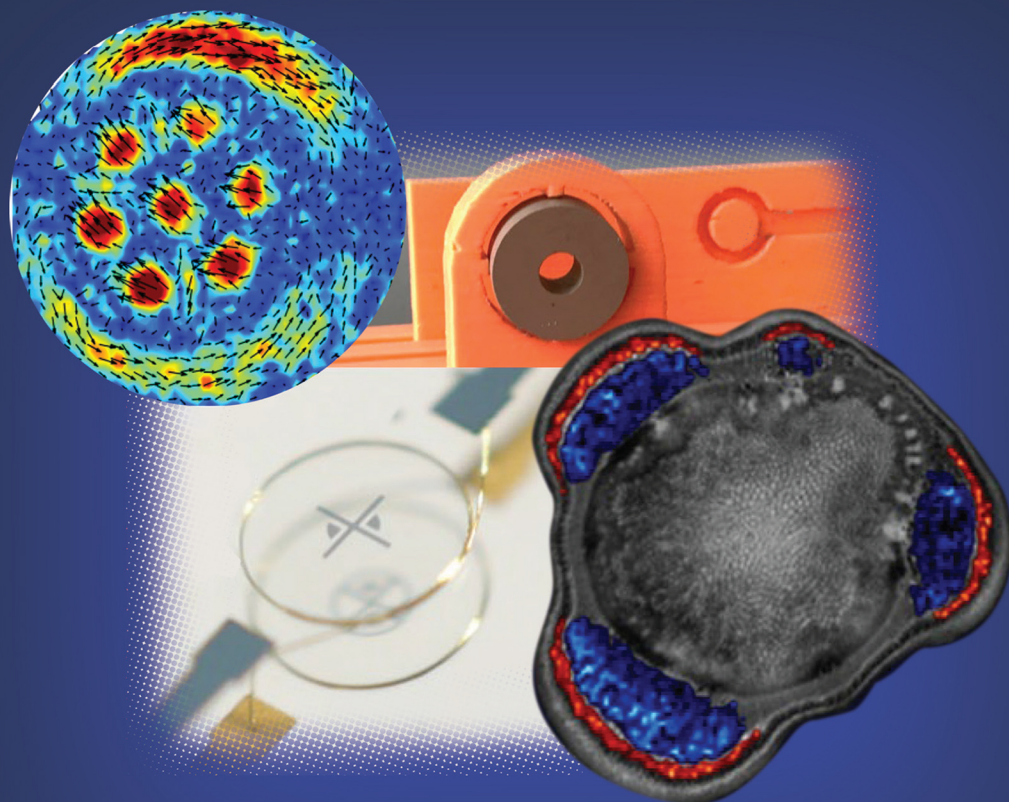Edited by Sabina Haber-Pohlmeier, Bernhard Blümich, and Luisa Ciobanu

Magnetic Resonance Microscopy

Instrumentation and Applications in Engineering, Life Science, and Energy Research

Magnetic Resonance Microscopy

Magnetic Resonance Microscopy

Instrumentation and Applications in Engineering, Life Science, and Energy Research

Edited by

Sabina Haber-Pohlmeier
RWTH Aachen

Bernhard Blümich
RWTH Aachen

Luisa Ciobanu
Paris

WILEY-VCH

Editors

Sabina Haber-Pohlmeier
RWTH Aachen University
Worringerweg 2
52074 Aachen
Germany

Bernhard Blümich
RWTH Aachen University
Worringerweg 2
52074 Aachen
Germany

Luisa Ciobanu
Point Courrier 156
Bat 145
91191 Gif sur Yvette
France

Cover Image: Courtesy of Denis Wypysek, Jan Korvink, Henk Van As, and Luisa Ciobanu

To my parents

Contents

Foreword

This book is the fourth in the Wiley-VCH series on *Magnetic Resonance Microscopy*, a series linked in spirit to the *International Conference on Magnetic Resonance Microscopy* (ICMRM). Winfried Kuhn and Bernhard Blümich organized the first meeting of this biannual conference in 1991 in Heidelberg, which led to the first book in this series. That Heidelberg meeting is also when Paul Callaghan burst upon the scene (with his student Yang Xia, who remains active in these meetings) with his new, but now classic, book *Principles of Nuclear Magnetic Resonance Microscopy* (Oxford University Press) – what timing! The wider appearance of magnetic gradient fields in the portfolio of magnetic resonance methods for imaging and studies of molecular transport phenomena was an exciting prospect. It motivated the still ongoing ICMRM conference series and the associated books, which summarize the progress in this field with chapters written by leading experts, among them Nobel Prize awardees Paul Lauterbur and Sir Peter Mansfield as well as Sir Paul Callaghan, who shaped that community like a force of nature from then on until his untimely death in 2012. Also, our brilliant colleague Robert Blinc from Slovenia attended the first ICMRM but had to leave early following an announcement during one of the sessions effectively saying "Professor Blinc, you are needed back in your country," at which Robert Blinc stood up and left to facilitate the independence of Slovenia from Socialist Federal Republic of Yugoslavia. We were witnessing the birth of a country, a unique experience for most of us. At the third meeting in Würzburg, the brave suggestion to hold a meeting in North America was accepted. Thus, the fourth meeting was in Albuquerque and ICMRM has now a truly international presence, having ventured as far away as Utsunomiya and Beijing. These meetings, originally dubbed the Heidelberg Meetings, have been at the forefront of amazing developments and accompanying applications of magnetic resonance. Despite the inclusion of the word *microscopy* in their name, they represent the much broader area of magnetic resonance with spatial resolution, which is expressed by the title of the second book from the Albuquerque meeting, *Spatially Resolved Magnetic Resonance*, as well as the organizing *Division of Spatially Resolved Magnetic Resonance* of the *AMPERE Society*. Thanks to the advances over three decades, we have micrometer spatial resolution in magnetic resonance imaging today, while in the early days the word microscopy was understood as a tool to see things hard to visualize just by eye. We believe the broad range of the science and applications of magnetic resonance represented in these meetings is unique to all science and the field displays no hint of imminent stagnation – welcome news to all of us. I would like to close this

Foreword with the observation that Bernhard Blümich, who with Winfried Kuhn founded these meetings 30 years ago, is still actively involved here as one of the editors of this book. I salute him for his continued contributions to the field and support of this conference.

Eiichi Fukushima
Albuquerque, 2021

Preface

Magnetic resonance microscopy (MRM) has focused on magnetic resonance imaging (MRI) applied to objects of smaller scale and higher spatial resolution for more than three decades. After the pioneering work by Eccles, Callaghan, Aguayo, Blackband, Johnson et al. in 1986, MRM quickly spread to, among other fields, chemistry, histology, and materials research. Since 1992, the edited book series *Magnetic Resonance Microscopy* has provided an important voice describing the latest developments in spatially resolved magnetic resonance methods and their applications far beyond the scope of medical diagnostics. An excellent introduction to MRM, focusing on the practical aspects of high magnetic fields and on the study of biological systems, was authored in 2017 by Luisa Ciobanu: *Microscopic Magnetic Resonance Imaging: A Practical Perspective* (Pan Stanford, Singapore, 2017). Our book complements this monograph by showing the use of MRM and related techniques in a much broader area and on a wider scale, which extends from chemical engineering to plant research and battery applications, highlighting the interdisciplinary nature of MRM.

The book opens with a section on hardware and methodology, covering aspects of micro-engineering, magnet technology, coil performance, and hyperpolarization to improve signal-to-noise ratio, a major bottleneck of MRM. Specific pulse sequences and developments in the field of mobile nuclear magnetic resonance are further topics of this first chapter. The following parts, 2 and 3, review essential processes such as filtration, multi-phase flows and transport, and a wide range of systems from biomarkers via single cells to plants and biofilms. Part 4 focuses on energy research, which is becoming increasingly important due to the globally growing environmental problems. It reports on battery types and their developments and how battery states can be recorded and characterized with MRM. However, we would like to point out to the reader that only a small sample of applications could be addressed in Chapters 1 to 4. Finally, the last chapter advocates that theory and applications should not be treated separately, because much can be gained from their complementarity.

The main aim of this book is to convince aspiring and established scientists from all fields that MRM is a versatile nuclear magnetic resonance (NMR) method that is capable of answering many questions from both the laboratory and everyday life. The book seeks to inspire a new readership from industries and innovative research directions to create synergies by adding MRM to their expertise.

The editors thank all the authors for contributing their invaluable knowledge to this book during a time challenged by COVID-19. Our thanks also go to the kind staff of the Wiley books department, who helped us with advice and support throughout the whole editing process.

<div align="right">

Sabina Haber-Pohlmeier
Luisa Ciobanu
Bernhard Blümich
Summer 2021

</div>

Part I

Developments in Hardware and Methods

1

Microengineering Improves MR Sensitivity

Neil MacKinnon, Jan G. Korvink, and Mazin Jouda

Institute of Microstructure Technology, Karlsruhe Institute of Technology, Eggenstein-Leopoldshafen, Germany

1.1   Introduction

Thirty years have passed since 1991 when Paul Callaghan published his book on magnetic resonance microscopy [1], and many works have subsequently appeared that have made numerous advances in this exciting field possible. Our goal for this chapter is to (informally) revisit some of Callaghan's analysis, to reflect on it, and then take account of some of the advances and insights that have been reported since then.

1.1.1   Comparative Electromagnetic Radiation Imaging

Paul Callaghan's book [1] is perhaps the first publication to consider magnetic resonance imaging (MRI) in the same light as optical microscopy. This will also be our starting point.

Until the advent of super-resolution microscopy, refractive optical microscopy was essentially a radiation scattering method, in which a beam of photons from an independent light source was sent on its way to scatter off objects, followed by traversal of the beam through a focusing objective on its way back to a detector, to thereby reveal the structure and composition of the scattering object. The limitations of this approach, in terms of resolution, is known as the Abbe limit $\delta = \lambda/(2\,n\,\sin\theta)$, where n is the refractive index, θ the half-angle of the spot subtended by the lens, and λ the radiation wavelength.

Using radio waves taken for convenience at 300 MHz, a thus interpreted refractive MRI system would have a resolution of ~500 mm, which is a dire prospect for applications of MRI. In a seminal paper, Mansfield et al. [2] reported on a form of nuclear magnetic resonance (NMR) diffraction, in which they considered a solid-state periodic lattice of spins in a macroscopically sized lattice, revealing diffraction patterns on the order of the lattice. As a follow-up to this idea, Blümler et al. [3] and Bernhard Blümich [4] reported (the latter in a paper dedicated to Paul Callaghan) on an interesting intertwining of concepts of the k-space vector of refractive MRI and the spatial periodicity of a lattice-like diffractive structure, further exploring diffractive imaging. Blümich's paper contains a few more gems worth discussing, but would distract us too far from the optical viewpoint we are considering here.

Near-field effects can be further exploited to increase the resolution of an imaging system. At optical wavelengths, one is hardly able to extend beyond 200 nm of resolution with currently available light sources. "The diffraction limit of light is 100 times the size of structures that cell

biologists study as they characterise events in organelles or membranes," Hari Schroff (NIH/ NIBIB) is quoted to say in [5], yet below 200 nm "is where most cellular action is," the author notes. The alternative is to avoid scattering as an imaging paradigm, instead, to image photon sources (also known as quantum emitters).

Interestingly, deep space astronomy always worked this way around by observing photon emitters, so that astronomers only consider objects that were once themselves sources of radiation, such as stars and their predecessors and descendants. In astronomy, the limit of resolution is therefore not dominated by the wavelength of the radiation, which can be very small when compared to the size and distance of the astronomical objects, but rather by the measuring instrument's principle of operation, its detection sensitivity, and in particular, its effective aperture.

When imaging radiation sources, such as single photon emitters in molecules, we now know that we can greatly improve on the Abbe limit, by about a factor of 10, especially when combined with techniques of stimulated emission and depletion, and one of the numerous variations based on fluorophore emission dynamics. These techniques, which have revolutionized cellular biology and won its inventor Stefan Hell the Nobel Prize in 2014, are of course not accessible to astronomers, who would have to wait too long for excitation signals to pass from observer to object and back again. But for cell biology this is not problematic. Although at currently ~30 nm, the resolution is still far from the desired 1 nm limit, advances in image processing present a feasible route to achieve further improvements. But the technique also raises some questions. Sample preparation is very difficult, and imaging is indirect as fluorophores have to be invasively attached to interesting molecules, almost certainly modifying their behavior.

Magnetic resonance microimaging is a noninvasive technique that is clearly more closely related to stimulated emission depletion (STED) microscopy than to conventional scattering light microscopy. A localized atomic nucleus' spin is a quantum absorber/emitter. By localizing the excitation field spatially or by frequency, a sub-selection of the spins in a sample can be prepared to absorb radiation. Further localization can ensure that emission of radiation energy is again sub-selected, for example along the geometrical intersection of two orthogonal manifold slices, the one for excitation, the other for emission. A range of further techniques, such as available through relaxation contrast, or phase accumulation, can again further sub-select spins before readout, thereby improving resolution in direct analogy to the techniques of fluorophore emission dynamics. Noninvasive Faraday-detected MRI has been reported down to ~3 μm resolution [6], which is already five orders of magnitude below the radiation wavelength. Nevertheless, even though MRI records radio frequency emissions, this is done almost exclusively through near-field interactions, i.e. by Faraday induction, and not from a beam or ray that requires a lens for focusing.

One of the limitations in NMR is certainly that a single quantum emission event is not yet readily observable as it would be in photonics, even though Dan Rugar showed that a single spin can be observed [7]. Thus all Faraday induction-acquired MRI images have to resort to averaging of a vast number of emission events, and over extended time, to yield useful information. If detection sensitivity were to be increased, fewer emitters could be used, and could perhaps be averaged over shorter times.

1.1.2   Limit of Detection

The statistical polarization level, i.e. that proportion of the total spin population that is available for quantum emission, is an additional cause of lack of signal. Proton spins for example are indistinguishable fermions, with a level occupation that follows

$$\langle N_i \rangle = \frac{1}{e^{(\varepsilon_i - \mu)/kT} \pm 1} \tag{1.1}$$

and which collapses to Maxwell–Boltzmann statistics when $e^{(\varepsilon_i - \mu)/kT} \gg 1$, because the energy of a proton flip $\gamma \hbar B_0 = 3.3 \times 10^{-25}$ J is tiny compared with the thermal energy $kT = 4.11 \times 10^{-21}$ J. Thus at typical equilibrium polarization levels at 11.7 T, a factor of only 10^{-4} in excess in population difference with respect to the Fermi level μ can contribute to the signal. An imaging voxel size is therefore principally limited by polarization, because we find – for microcoils at their limit of detection – a sample containing around 10^{13} spins is needed to form an observable signal. Clearly, this sets a lower concentration limit once the voxel size is specified. For example, at the average size of a single eukaryotic cell of $(10 \, \mu m)^3$, containing the required nuclei, implies a concentration of at least 1.66 µM. By increasing polarization, the voxel size is thus principally reduced, or the lower concentration limit is reduced, which could be achieved by resorting to out-of-equilibrium polarization techniques such as parahydrogen-induced polarization (PHiP), signal amplification by reversible exchange (SABRE), or dynamic nuclear polarization (DNP), all of which are rather hard to perform noninvasively, and hard to selectively localize too. We will return to this point shortly. One of the key advantages of MR-based microscopy is the ability to noninvasively reveal molecular composition, correlated with morphology. From the perspective of biological systems, this can be leveraged to monitor, for example, spatially resolved metabolism. To estimate the best achievable spatial resolution (voxel size), signal-to-noise ratio (SNR) should be considered in the context of the metabolically active system. Key parameters are the molecule abundances (concentrations) and timescale that are targeted. Consider a spatially resolved fluxomic investigation: can one estimate a realistic MRI spatial resolution taking into consideration the expected biological dynamics? Alternatively, what is the smallest biological structure with which metabolic flux can be measured – thus, is it possible to monitor flux at the level of an organelle, single cell, cell cluster, or tissue?

Water is the most abundant molecule in biosystems and can be used as a useful reference from which scaling based on metabolite concentrations can be made. Using only the physical volume of a water molecule (0.03 nm^3), and an optimistic limit of detection (LOD) of 10^{13} spins, then an order of magnitude estimate of the smallest voxel is 0.1 pl (approximately 4.5 µm isotropic resolution). This is approximately the volume of a single red blood cell. Intracellular metabolite concentrations vary over several orders of magnitude, with the most abundant molecules typically in the tens of millimolar regime. The best-case scenario scaling factor is then 10^4 relative to water (assuming [water] = 55 M), and thus the smallest voxel volume increases to 1000 pl (100 µm isotropic resolution). For reference, this would correspond to 10 000 red blood cells or 2 fat cells (volume 600 pl per cell). Can the resolution be improved by signal averaging as a means to enhance SNR? Assuming metabolism is active during the measurement then one must consider the turnover rate of the target metabolite(s) relative to the time over which signal averaging is performed. Enzyme catalytic (second-order) rate constants span several orders of magnitude ($k_{cat}/K_M \sim 10^1 - 10^9$ s^{-1} M^{-1}), with a median of $\sim 10^5$ s^{-1} M^{-1} [8]. If the metabolite concentration is 100 mM, then the metabolite will encounter the "median enzyme" with a rate of 10^4 s^{-1}. At this concentration and a volume of 1000 pl, the metabolite concentration would drop below the LOD ($\sim$10 mM) in 6000 days giving more than sufficient time for signal averaging. At the diffusion

limit $10^9\,\mathrm{s}^{-1}\,\mathrm{M}^{-1}$ then, 6 days are required before the signal is not observable. This rough estimate takes many liberties in the assumptions (catabolic and anabolic reactions, multiple pathways, enzyme performance, cell cycle, etc. are neglected) and simply suggests that signal averaging is reasonable, most likely limited by technical factors like long-term sample maintenance and spectral resolution accounting for magnetic susceptibility effects. Interesting, it is revealed that single cell metabolic monitoring is challenging yet possible as long as (i) large cells are selected; (ii) the metabolite is among the most abundant in the cell at millimolar concentration; and (iii) the cell can be maintained in an active state during the measurement. Spatial resolution and/or detected concentrations can be improved if hyperpolarization strategies are used where the effective LOD can be improved by orders of magnitude with percent (instead of ppm) levels of polarization. Using the same set of assumptions, now with percent levels of polarization, it is estimated that on the order of a few minutes is required ("median enzyme" kinetics) before the observation of hyperpolarized metabolic products, consistent with observations [9].

Currently, the only other means known to further increase resolution in cell biology, is based on the higher sensitivity and simultaneously higher localization that arises from proximity to the spin. When detector and spin are separated on the order of 1 nm, the dipolar coupling is strong. The techniques, such as magnetic resonance force microscopy [7], or nitrogen-vacancy (NV) centers in nanodiamonds [10], are either invasive (magnetic resonance force microscope [MRFM]) or require similar sample preparation as for STED (NV centers), namely to introduce a mobile quantum emitter that is tagged to a molecule to wander through the cell.

1.1.3   Limit of Imaging Resolution

Paul Callaghan [1] and others [11–14] showed that the imaging resolution of MR microscopy is fundamentally limited by three factors: the diffusion coefficient of molecules within the sample, the line broadening due to magnetic susceptibility effects, and the specified SNR per voxel. While the limits placed by the first two factors can be pushed by stronger field gradients and dedicated pulse sequences [15], the rather poor SNR of the MR signal remains as the ultimate fundamental limit of resolution. This can be clearly seen from the following equation [16,17], which summarizes the factors that determine the achievable resolution for a specified SNR of the image:

$$V_{\mathrm{voxel}} \propto \frac{d}{\sqrt{t_{\mathrm{acq}}} \cdot B_0^{7/4}}, \tag{1.2}$$

where V_{voxel} is the voxel volume, d is the coil diameter, t_{acq} is the total acquisition time, and B_0 is the field strength. According to this equation, maintaining the image SNR while, for instance, halving the isotropic resolution (reducing the voxel volume by a factor of 8) necessitates either miniaturizing the coil by a factor of 8, increasing the acquisition time by a factor of 64, or increasing the B_0 field by a factor of 3.28. This explains why high-resolution MR images take excruciatingly long to acquire, and why most groups decrease coil diameter. However, at room temperature, coil diameter cannot be reduced indefinitely without disadvantageously increasing coil resistance, so that quality factor Q will ultimately limit this strategy.

1.2 High Resolution From Enhanced Sensitivity

### 1.2.1 Coil Miniaturization

In Equation 1.2, d represents the sensitivity of the NMR detector, which has been proven to increase with decreasing d [18]. Numerous reports have been published on how to improve the NMR detection sensitivity by miniaturizing the detection coil [19–22]. The vast majority of those papers targeted NMR spectroscopy applications, and far fewer talked about microscopy [23–25]. One of the papers that targeted both applications though is the work reported by [26]. In this paper a novel high-resolution NMR/MRI Helmholtz microcoil was introduced (Figure 1.1). The coil that was manufactured using a combination of standard and home-developed micro fabrication technologies featured an extremely user-friendly sample-handling approach that allows easy loading/unloading of the sample.

The coil was manufactured by stacking three layers, the top and the bottom of which are made of glass, each featuring a wire-bonded 1.5-winding coil using a 25-μm diameter copper wire. The coils were encapsulated in SU-8 epoxy-based photoresist. The glass layers also contained copper traces for the feed and return paths of the current. These layers were spaced by a poly(methyl methacrylate) (PMMA) layer, which was U-shaped to allow the sample-handling microfluidic chip to slide in the sensor. The Helmholtz microcoil was designed and optimized to achieve an extremely uniform B_1 field (92% ratio of signal intensity at flip angles of 810/90) while maintaining the high B_0 homogeneity (1.79 Hz achieved linewidth of a water sample).

The exceptional performance of the microcoil in terms of B_1 uniformity and local field homogeneity allowed high-resolution microimaging. Figure 1.2 shows the optical (left) and MR (right) microimages of a deionized water sample of 154 nl volume. The sample contains 50-μm diameter polymer beads to show some contrast. The MR image that is a sum of 80 acquisition was recorded over a total scan time of 11 h, 22 min, and 40 s. With a matrix size of 256×256 and covering a 2.5×2.5 mm field of view (FoV), the MR image exhibited an in-plane resolution of 10×10 μm for a slice with a 100-μm thickness.
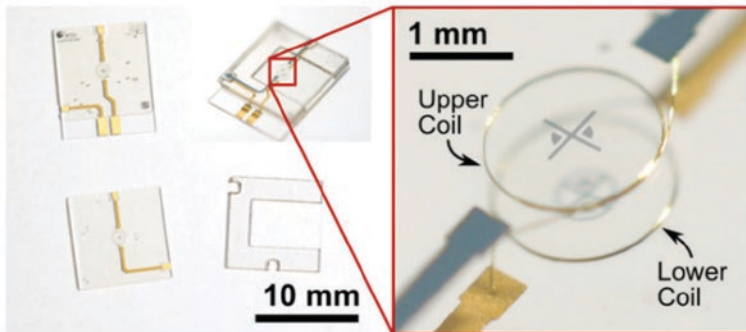
Figure 1.1 A micro Helmholtz coil manufactured using a mixture of standard and home-developed micro-manufacturing technologies. [26] N. Spengler et al. (2014), figure 04 [p.05]/with permission from IOP Publishing Ltd.
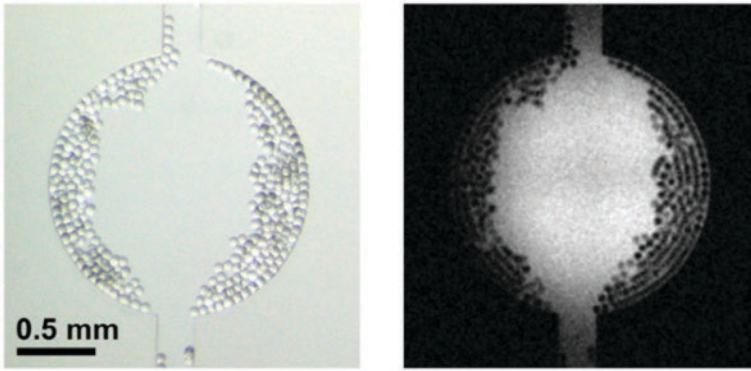
Figure 1.2   MR microimaging of a 154-nl deionized water sample with 50-µm diameter polymer beads. (left) Optical micrograph. (right) MR image. [26] N. Spengler et al. (2014), figure 10 [p.07]/with permission from IOP Publishing Ltd.

### 1.2.2   The Lenz Lens: A Tool to Boost Sensitivity

The quest for higher coil sensitivity, SNRcoil $\propto$ B1/(iR), made researchers invest huge efforts in the design and optimization of the NMR detector. These efforts resulted in numerous publications covering a wide diversity of coil geometries and applications. Nevertheless, none of these efforts went beyond two major pathways: (i) optimizing the coil geometry to better confine the sample and thus achieve a higher filling factor, which, in turn, results in a higher B_1 per unit current seen by the sample; and (ii) reducing coil resistance, R, and thus its noise contribution either by a careful selection of coil materials, or by cooling the coil windings. In certain cases, however, these strategies might not be applicable as, for example, if one wants to study the inner body parts. For this particular case, implantable inductively coupled inductor-capacitor (LC) resonators have been shown to enhance the imaging SNR remarkably [27–32]. Nevertheless, despite their advantages, LC resonators suffer from limited frequency accessibility due to their narrowband nature, which originates from the resonance phenomena, and the difficulty in tunability due to their sensitivity to both the sample and the pick-up coil [33].

An alternative to the LC resonator is the Lenz lens (LL) shown in Figure 1.3. The LL consists of two electrically connected loops: the inner and outer loop, where the outer loop collects the magnetic flux of the pick-up coil and converts it to a current. As this current passes through the inner loop of the LL, it generates a larger magnetic field in the sample than the field that would otherwise be produced by the pick-up coil only. The LL, though less powerful in terms of field amplification compared with the LC resonator, is superior to it in terms of tunability and wide frequency accessibility [33]. Figure 1.4 depicts a simulated comparison of the SNR as the coil geometry increases with respect to the sample volume of a single-loop planar wired coil (blue), a single-loop planar coil with a LL (red), and a single-loop planar coil with an LC resonator (green).

The concept of LL was applied by Spengler et al. [34] to his previously reported NMR micro Helmholtz detector. Figure 1.5 shows an LL with 1 mm outer diameter and 0.2 mm inner diameter inserted inside the micro Helmholtz LL2 coil. In the paper, four different lenses were tested, namely plate lenses LL1 and LL2 with inner diameters of 0.2 mm and 0.4 mm, respectively, and wire lenses LL3 and LL4 with inner diameters of 0.2 mm and 0.4 mm, respectively. The performance of the lenses was evaluated via a series of MRI spin echo imaging experiments on a
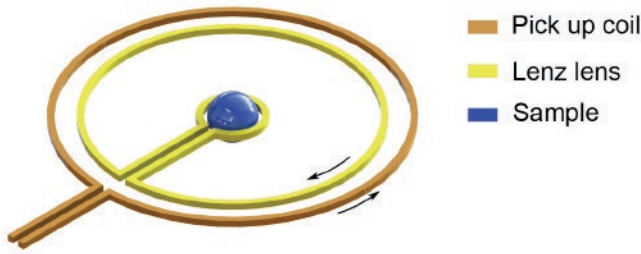
Figure 1.3 The Lenz lens (LL) collects the magnetic flux of the pick-up coil and focuses it into the sample region resulting in an enhanced sensitivity of the measurement.
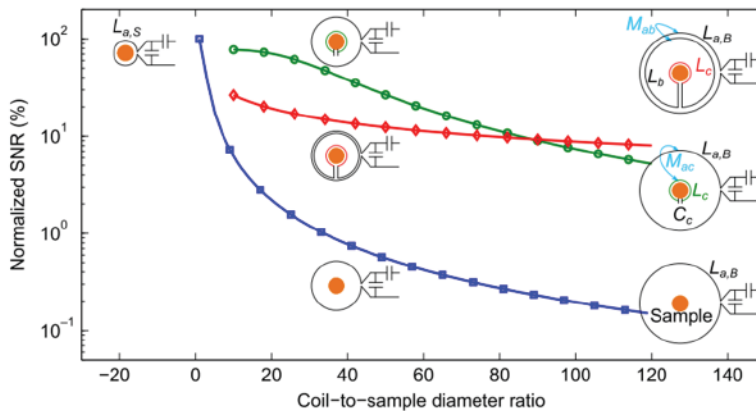

Figure 1.4 A comparison of the LL performance versus the LC resonator for a planar single-loop pick-up coil. The first point of the blue curve is the optimum situation where the coil geometry perfectly matches the sample volume (coil-to-sample diameter ratio = 1). As the coil geometry increases in comparison with the sample volume the SNR decreases. In this suboptimal situation, the SNR can be improved by using either an LC resonator (green curve) or a LL (red curve). In this figure, $L_{a,S}$ is the inductance of the small pick-up coil, $L_{a,B}$ is the inductance of a big pick-up coil, L_b is the inductance of the outer loop of the LL, L_c is the inductance of the inner loop of the LL, and M is the mutual inductance.

deionized water sample. All experiments were preceded by flip angle adjustment routines to ensure that all the measurements are conducted at the same flip angle, namely 90°. Figure 1.6 calculates the SNR enhancement due to the various lenses (LL1–LL4) and compares it with the reference SNR of the micro Helmholtz coil without lenses (the red curve). According to the results, exploiting LLs can significantly enhance the coil sensitivity and thus the achievable imaging resolution. The SNR enhancement varies largely with the inner diameter of the lens (increases as the inner diameter decreases) but changes slightly with the topology used (plate/wire). The maximum SNR enhancement reported in the paper was 2.8, which would allow reducing the voxel volume by 64% (reducing the voxel length by 29%) while maintaining the acquisition time and the SNR per voxel unchanged. A system that combines the concepts of both the LL and the LC resonator has been introduced by Kamberger et al. [35]. The so-called resonant LL benefits from the field-focusing feature of the LL and the signal amplification advantage due to resonance. The resonant LL was integrated with an MR-compatible incubation platform designed to cultivate organotypic hippocampal slice cultures (OHSCs), to perform in vitro MR microscopy of brain tissues. The wireless LL was purposely employed to avoid the direct
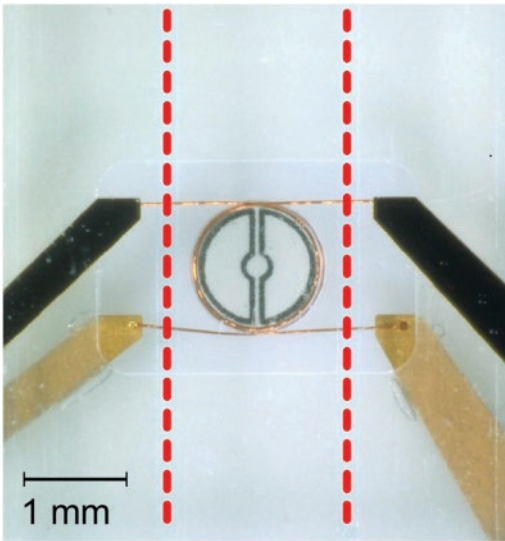
Figure 1.5 A Helmholtz micro coil with a wire Lenz lens. [33] Nils Spengler et al. (2017), figure 03[p.008]/Public Library of Science (PLoS)/CC BY 4.
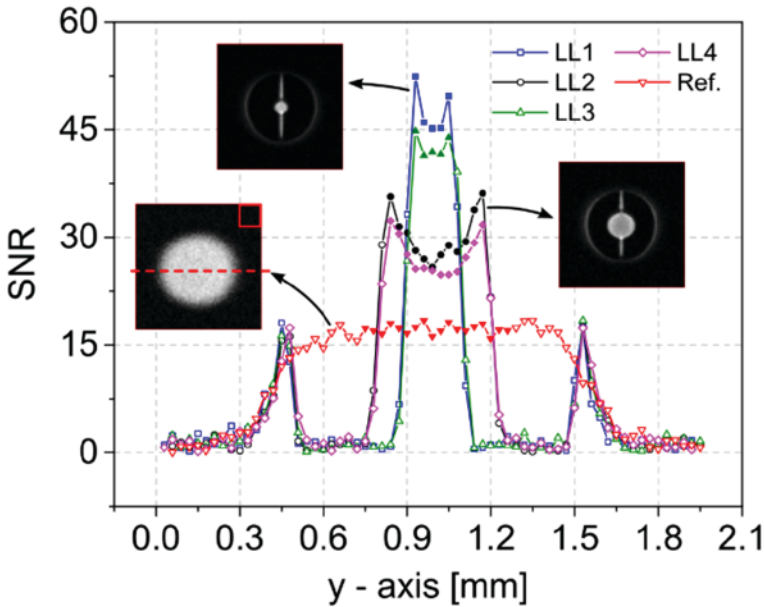
Figure 1.6 Sensitivity enhancement of the micro Helmholtz coil due to Lenz lenses. The red curve indicates the reference signal-to-noise ratio (SNR) of the Helmholtz coil along the center line of the image when no Lenz lenses are used. The other curves show how the use of Lenz lenses boosts SNR of the sample region in the inner loop of the lens. The SNR enhancement ranges from 1.6- to 2.8-fold. [34] Nils Spengler et al. (2017), figure S1/Public Library of Science (PLoS)/CC BY 4.0.

connections of wired RF coils, thereby giving the incubation platform more flexibility and freedom. Moreover and more importantly, avoiding wired coils reduces the number of different-materials interfaces, which consequently diminishes the susceptibility-mismatch-based imaging artifacts. In fact, the latter issue is an extremely important aspect when considering microscopy. For this reason, the LL introduced in [35] was carefully designed and manufactured by patterning thin copper tracks on a slender polymer foil so as to minimize the susceptibility-mismatch effects. The proposed LL was tested in a 9.4-T horizontal bore Bruker small animal MRI scanner. The scanner is equipped with a 72-mm-diameter volume coil. Three measurement scenarios were used to enable a comprehensive comparison of the performance. These scenarios are:

1) MR imaging using the bare volume coil without any add-ons. This measurement served as the baseline to which the other scenarios can be compared.
2) MR imaging with a broadband nonresonant LL integrated with the incubation platform and inserted in the volume coil.
3) MR imaging of a resonant LL tuned, by a discrete capacitor, at the Larmor frequency and integrated into the incubation platform.

In all experiments, a T_1-weighted Flash sequence was applied to obtain an MR image of a mouse brain slice with a 0.5-mm thickness and an in-plane resolution of 100×100 μm from 16 averages over 8 min. The results, as demonstrated in Figure 1.7, show a significant enhancement in the
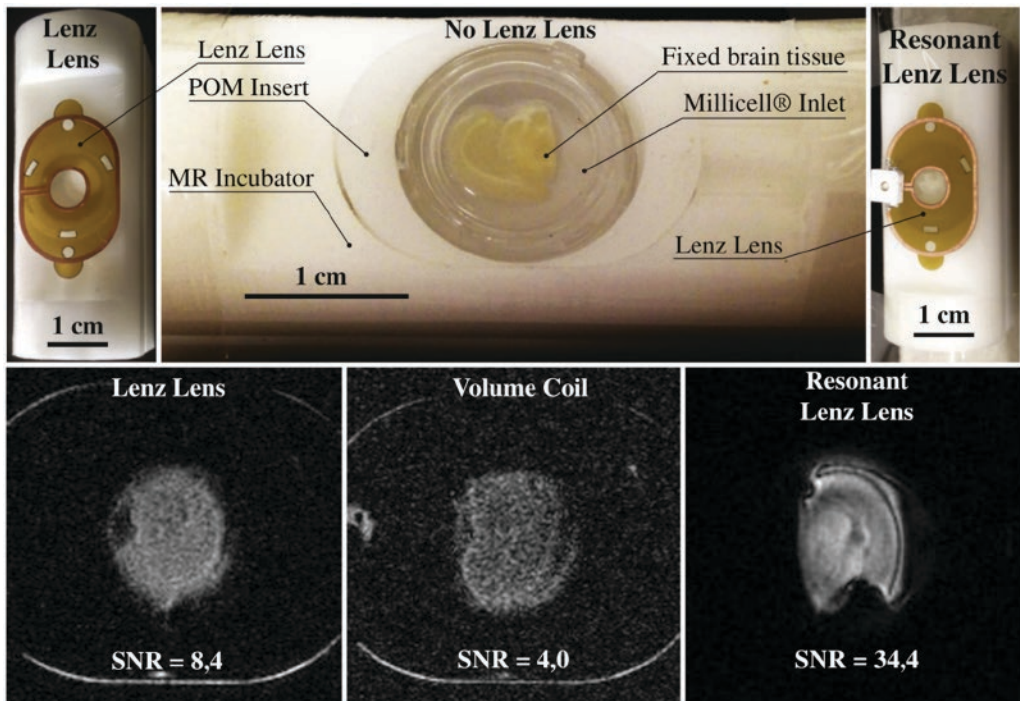
Figure 1.7 Top: Magnetic resonance (MR) compatible incubation platform for cultivating mouse brain slices. The platform was integrated with a broadband nonresonant Lenz lense (LL) (left), and a resonant LL (right). Bottom: MR images of a brain slice using the Bruker volume coil (middle), the broadband LL (left), and the resonant LL (right). [35] R. Kamberger et al. (2018), figure 06[p.13]/with permission from Elsevier.

imaging SNR due to LLs. More specifically, a broadband nonresonant LL achieved more than double the SNR of the volume coil, while an 8.5-fold SNR enhancement was obtained by the resonant LL.

1.3 MR Microscopy and Neurotechnologies

"One cubic millimeter of cerebral cortex contains roughly 50,000 neurons, each of which establishes approximately 6,000 synapses with neighbouring cells" [36]. Thus any attempt to shed light on brain function using MRI or NMR will necessarily have to apply MR microscopy. A number of aspects, especially in brain research, are amenable to MR, especially those associated with possible brain interventions, and those involved in functional magnetic resonance imaging (fMRI) of the brain. We briefly consider these aspects next.

1.3.1 Tissue Scaffolds and Implants

Neurotechnologies rely on long-term implantable technical systems, in which technical materials come into direct contact with brain tissue, which mainly consists of neurons and a permeating vasculature. Two questions are of central concern:

1) Do neurons permit intimate contact with the technical system?
2) Do the materials of the technical system disturb subsequent MRI?

The realization that carbon, despite its hardness, is readily accepted by many cell types, also by stem cells, led to the exploration of microstructurable carbon as a tissue scaffold for studies in cell migration, network formation, and cell response [37]. In this study, an aqueous cryogel was steadily cooled, causing ice nucleation and crystal growth with morphological control, which upon thawing remained separated so that after drying a 3D polymer network remained. The network was pyrolyzed to yield an interconnected 3D carbon lattice, which in turn could be populated by neuronal stem cells, which allowed medium- to long-term studies of cell viability, confirmed by gradient echo MRI, see Figure 1.8.

Moreover, the low susceptibility to warping of the magnetic field caused by the carbon scaffold at 11.74 T opened the door for the exploration of carbon as a neuronal implant [38]. In this study, the authors produced carbon brain implant microelectrodes on Kapton foil, by lithographically structuring a photopolymer followed by pyrolysis and embedding in durimine before release. The implants were then investigated for their MR properties, including force-induced vibrations using a specially constructed dynamic force sensitive probe head [39]. Compared with platinum electrodes, which sufficiently warped the MRI signal coming from neighboring voxels, carbon electrodes permitted the acquisition of unwrapped images right up to the microelectrodes, thus paving the way for studies in postoperation tissue recovery and wound healing.

1.3.2 The Case of Epileptogenesis: Ex Situ Brain Slices and in Situ Histology

Brain-implanted microelectrodes target devastating diseases such as Parkinsons or epilepsy, and one of the primary questions in the field is whether it is possible to use noninvasive MRI to diagnose the disease, monitor recovery and temporal evolution of disease progress, and confirm correct system function of the implant. The hope is to translate diagnostic findings from mouse

models to humans, despite certain differences, but with the benefit of using higher fields and hence higher-resolution techniques on model organisms than are generally available for humans. The gold standard for epileptogenesis is a kainate-initiated temporal lobe epilepsy mouse model established by Bouilleret et al. [40], for which a dedicated MR-compatible tissue slice environment was developed [35]. In this device, a freshly extracted brain slice 5 mm diameter, 500 μm thickness is maintained at physiological conditions (36°C, perfused, oxygenated) during MRI (Figure 1.7). Additional studies, which tracked the morphological changes of the brain slice over longer timeframes, were performed using a cryogenic vendor-supplied small animal coil [41], for the first time yielding confirmation of histological correlates with various MRI modalities. Using the same cryo-imaging coil, translation of these techniques to the full animal model yielded a comprehensive picture of the disease progression [42] and established a number of new measurement and postprocessing techniques, including high-resolution diffusion tensor imaging, see Figures 1.9 and 1.10.

1.4   Augmented MR Microscopy

In situations in which microscopy is desired of objects that themselves have small dimensions, then there is an MR sensitivity advantage when using micro detectors. The challenge of sample handling at these dimensions, often achieved by microfluidic systems, can be turned into a feature when one considers the library of lab-on-a-chip (LOC) technologies already available, offering additional degrees of freedom in terms of sample management and interaction. Integration of NMR and microfluidics has continued to advance, starting from the earliest microcoil reports [43,44] to recent efforts taking advantage of LOC principles to enable
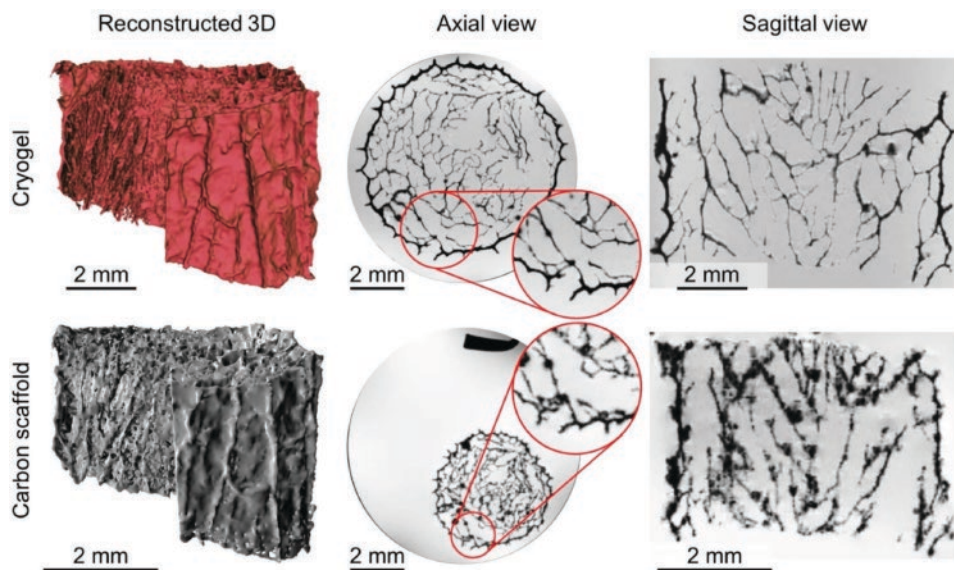
Figure 1.8   Porosity and connectivity analysis of a neuronal scaffold using magnetic resonance imaging microscopy, comparing a cryogel with its pyrolized and hence shrunk carbon counterpart. [37] Erwin Fuhrer et al. (2017), figure 02[p.03]/with permission from John Wiley & Sons, Inc.
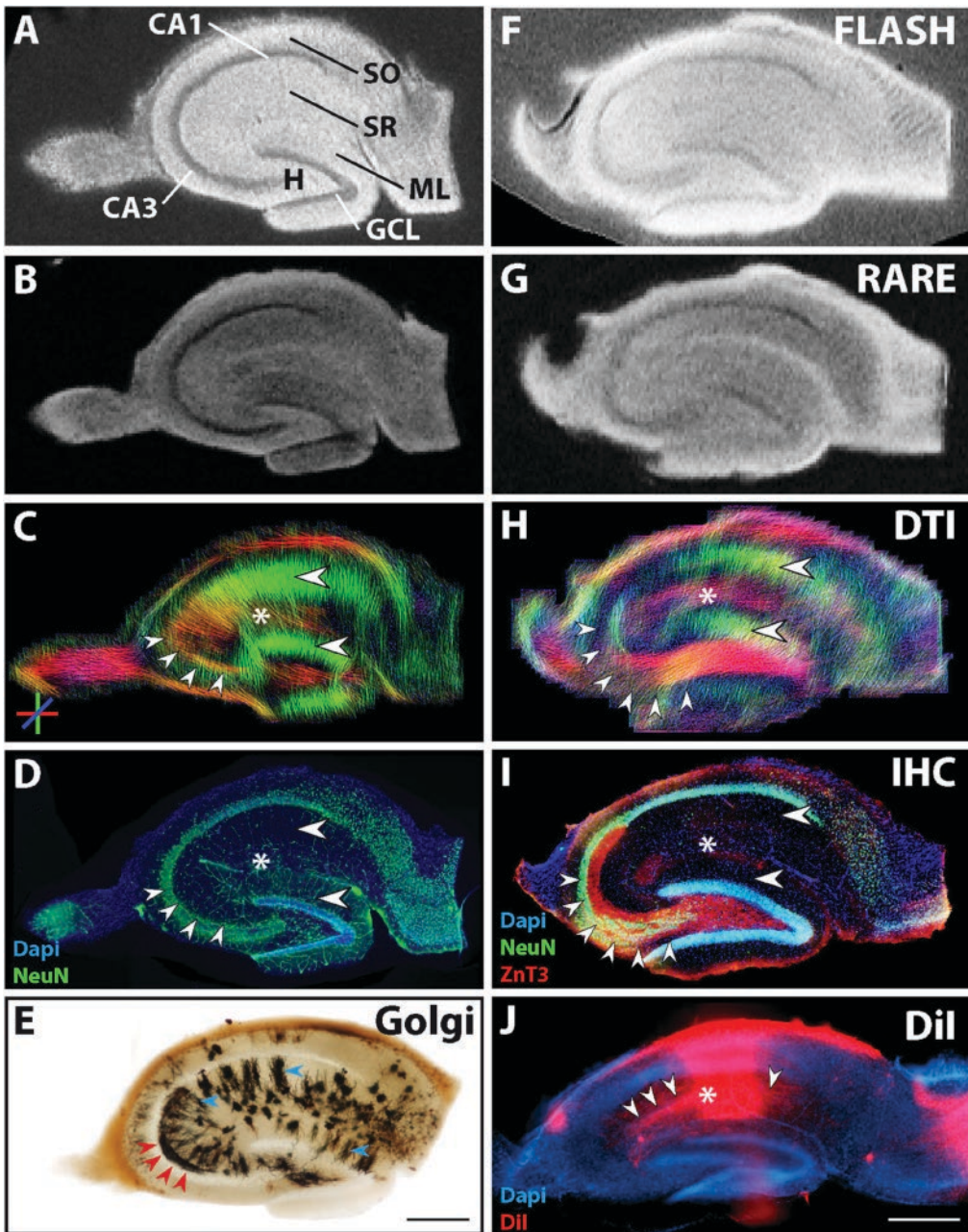
Figure 1.9 Magnetic resonance (MR) and histological images of fixed hippocampal sections of two control animals (Section 1: A–D, with an adjacent section used for Golgi staining: E; Section 2: F–I). (A, B, F, G) Structural magnetic resonance imaging (MRI) depicts the main neuronal cell layers and tissue architecture. Comparison of diffusion tractography images (C, H) to corresponding NeuN and ZnT3 immunostaining (D, I) shows that regions containing parallel extending dendrites of principal neurons evoke corresponding diffusion-weighted imaging (DWI) streamlines. (E) Golgi staining of an adjacent section depicts the localization and orientation of principal cell dendrites (blue arrowheads in SR and ML) and parts of mossy fibers in CA3 (red arrowheads). (J) DiI crystal placed into the CA1 stratum radiatum, showing the orientation of CA1 pyramidal cells as well as of innervating CA3 Schaffer collaterals (asterisk and arrowheads, respectively). Scale bar: 500 µm. [41] Katharina Göbel-Guéniot et al. (2020), figure 02[p.06]/Frontiers Media S.A./CC BY 4.0.
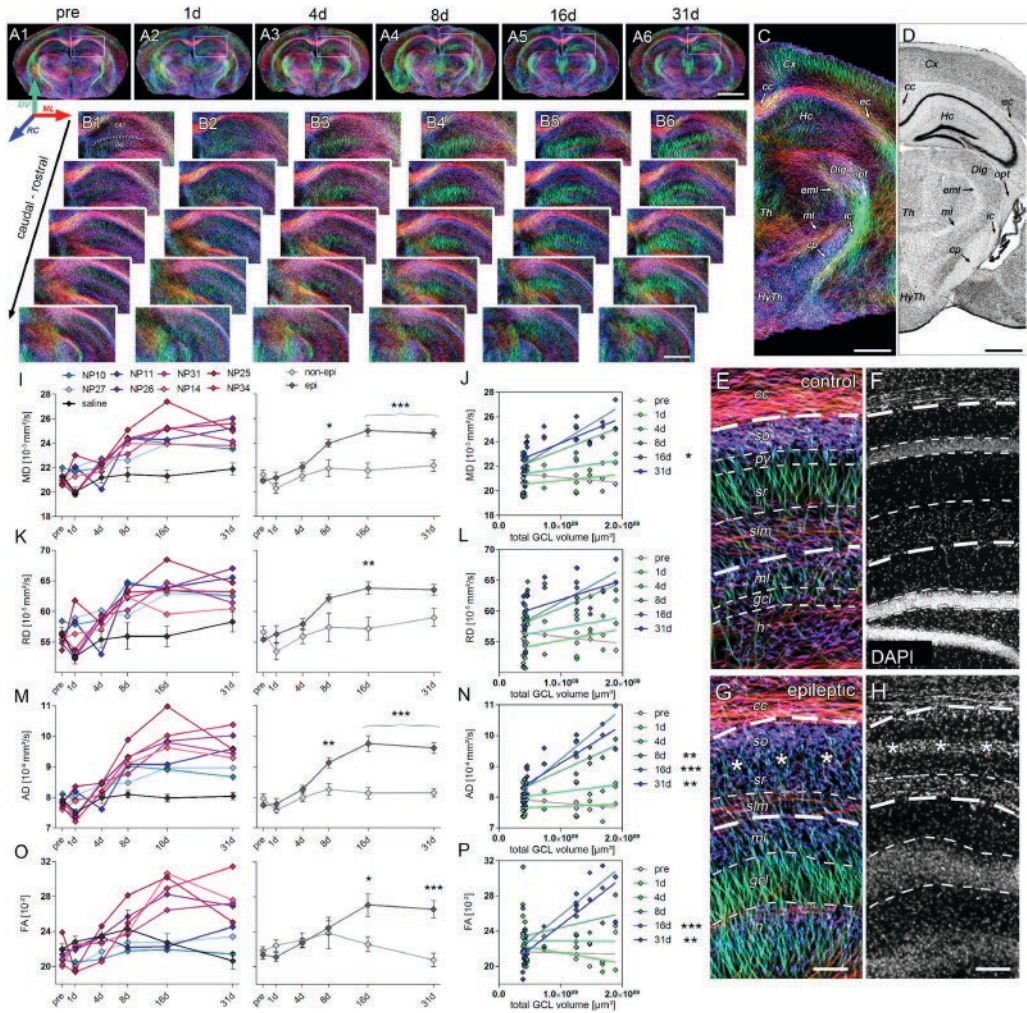
Figure 1.10 Microstructural reorganization quantified by diffusion-weighted imaging (DWI) during epileptogenesis predicts disease progression. (A1–6) Representative coronal sections from diffusion-weighted tractography at different time points during epileptogenesis (before injection = pre; 1 day, 4 days, 7 days, 14 days, and 31 days following SE). (B1–6) Enlarged images. (C–D) Representative tractography image and a Nissl-stained section of corresponding brain regions for anatomical comparison. Computed fibers relate to major axonal pathways and brain regions exhibiting highly oriented dendrites (cc, corpus callosum). (E, G) Enlarged tractography images demonstrating the distinct orientation of streamlines in different hippocampal layers. (F, H) Corresponding 4′,6-diamidino-2-phenylindole (DAPI)-stained sections. Scale bars in A, 2 mm; B–D, 500 mm; H (left), 100 mm (I, K, M, O). Quantitative analysis of DWI metrics in the dentate gyrus (DG), plotted for individual mice (left panel; controls, black, n = 5; kainate-injected animals color-coded) and for groups during epileptogenesis. [42] Philipp Janz et al. (2017), figure 05[p.10]/eLife Sciences Publications Ltd./CC BY 4.0.

microfluidic-based perfusion [35,45–49], electrochemistry [50], and hyperpolarization [51–53]. As discussed extensively in this chapter, micro-NMR coupled with MR microscopy is established and continues to evolve, with one branch of this evolution now extending toward fully exploring the augmented micro-MR system to further enhance the applicability of MR microscopy.

1.4.1 Perfusion

Perfusion can be considered a subclass of flow-based methods. In the context of this discussion, the definition of perfusion is relaxed slightly to include the passage of a fluid through microfluidic systems for the purpose of transporting nutrients and waste. Therefore, such systems can be used to maintain biological samples under conditions conducive to normal behavior, enabling long-term measurements of the system under normal and stimulated situations. Systems may include cell populations/layers/clusters and may increase in complexity up to tissue slices, organ-on-a-chip, and small organisms. Long-term measurement of such systems while using MR-compatible technical systems enables spatially resolved, longitudinal monitoring of morphology as a function of interesting stresses.

Starting from spectroscopy, perfusion-enabled microfluidic devices for long-term monitoring of biological systems have been used to monitor metabolic flux. Kalfe et al. [49] monitored a single tumor spheroid with diameter 500 μm over 24 h to characterize the transition from oxidative to glycolytic metabolism. Given the small volumes, it is important to ensure that the metabolic activity is reflective of the actual biological system and not perturbed, for example, by a lack of oxygen in the culture medium. This issue has been directly addressed by Yilmaz and Utz [47], who used a gas permeable membrane in combination with a micro-stripline [46] to ensure adequate oxygen supply for in situ cell culture NMR spectroscopy. Using 3D printing to produce MR-compatible microfluidic systems Montinaro et al. [45], demonstrated spectroscopy of small organisms, achieving detection volumes of 100 pl and therefore substructure spectroscopy of *Caenorhabditis elegans* in their work.

Incubator systems have been implemented for improved tissue slice MR microscopy. To enable long-term microscopy of a biologically viable tissue, incubator systems must not only manage perfusion but also gas concentration and temperature control. Flint et al. [48]. developed such an incubator system compatible with a 600-MHz NMR spectrometer. They demonstrated diffusion-weighted imaging of rat cortical slices with 31.25 μm isotropic resolution (1.5 h measurement time) over 21 h. The challenge for soft tissue incubation in vertical bore NMR systems is preventing tissue deformation caused by gravity. This can be addressed, for example, by physically clamping the tissue taking care not to unnecessarily perturb the tissue function. This challenge can be circumvented by ensuring gravity is perpendicular to the tissue surface, easily achieved in horizontal bore systems. Kamberger et al. [35] implemented an incubator for mouse brain slice imaging under this condition, with the added feature of a LL for magnetic field-focusing and improved SNR [33]. Using a 9.4-T MRI system, T_1-weighted images could be obtained in 8 min with 0.5 mm slice thickness and in-plane resolution of 0.1×0.1 mm, importantly, with a factor of 10 improved SNR yielded by the LL (Figure 1.7). In a clever use of capillary forces, tissue–air interfaces perpendicular to B_0 were avoided by allowing the perfusion medium to slightly overfill the tissue chamber thereby eliminating magnetic susceptibility-induced imaging artifacts.

1.4.2 Electrochemistry

The microfluidic LOC and micro total analysis system (μTAS) communities have recognized the added value of implementing electro-manipulation capabilities. From the perspective of biological samples, the electrical degree of freedom enables new methods for sample manipulation and sample analysis [54]. From a chemical perspective, electric fields can be used for selective analyte transport or to drive electrochemical reactions. Simultaneous integration with microscopy has

the potential to spatially localize the electro-response of the system, noninvasively and label-free in the case of MR microscopy.

MR-coupled electrochemical methods are often used to study electrophoretic behavior of electrolytes [55–57]. In these experiments, the electrodes used to generate the electric field are located outside of the NMR-sensitive volume. In the case of monitoring electrochemical reactions, it would be advantageous to localize the reaction within or in the immediate vicinity of the NMR detection volume. This has been demonstrated outside of the microfluidic domain, with recent efforts aiming to retain high-resolution NMR spectra at high magnetic fields using standard sample tubes [58–61]. NMR-compatible microfluidic systems with integrated electrodes are rare; in one example, a digital microfluidic approach has been demonstrated as a means to manipulate droplets and deliver sample to the NMR detection volume [62,63]. An in situ electrochemical system has recently been reported, including an analysis of the appropriate electrode properties that maintain acceptable NMR spectral resolution [50] (Figure 1.11). In this report, MR microscopy is additionally demonstrated, although in this case for the purpose of B_0 and B_1 field characterization.

1.4.3 Hyperpolarization

Micro-NMR detectors feature a sensitivity advantage for mass-limited samples, yet still suffer in terms of absolute sensitivity as dictated by the total number of signal-contributing spins in the sample. Hyperpolarization methods successfully circumvent this limitation and have proven extremely fruitful under "standard" NMR measurement conditions. Extending these capabilities to the microfluidic NMR domain was inevitable, yet progress has not been as dramatic as in
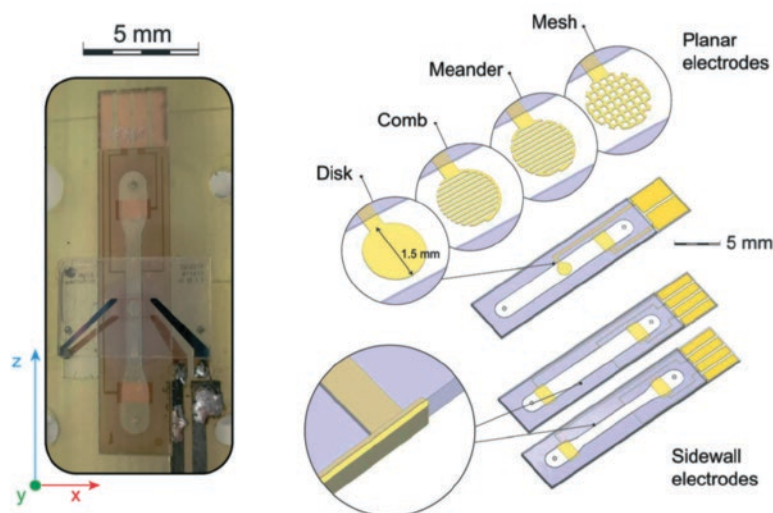
Figure 1.11 Photograph of a microfluidic insert featuring integrated electrodes (left) compatible with the micro Helmholtz detector. A variety of electrode geometries are possible from a fabrication standpoint (right), but care must be taken when considering MR compatibility. Davoodi et al. (2020). An NMR-compatible microfluidic platform enabling in situ electrochemistry. Lab on a Chip, 20(17), 3202–3212. Licensed under CC-BY-NC 3.0.